Phase retrieval in coherent diffraction from Cu_3Au antiphase domains

J. A. Pitney[a], I. A. Vartaniants[b], and I. K. Robinson[a]

[a]Department of Physics, University of Illinois, 1110 W Green St., Urbana, Illinois, USA
[b]Institute of Crystallography RAS, PO Box 12, 111395, Moscow, Russia

ABSTRACT

Below its critical temperature (668K), crystals of the binary alloy Cu_3Au consist of antiphase domains with a length scale determined by growth conditions and annealing history. Superstructure Bragg reflections indicate the extent of long-range ordering of the domains. The use of a coherent beam causes these superstructure peaks to have the appearance of speckles, which have a size determined by the size of the beam. The speckles result from a scattering process with no ensemble averaging and thus describe the specific microscopic arrangement of the domains within the illuminated volume of the sample. However, in real experiments only the diffracted beam intensity can be measured while all phase information is lost. This problem is overcome in conventional holography by the construction of a reference wave; however, the special requirements of x-ray optical design have precluded the direct application of this approach, and so the use of numerical analysis is required. Iterative methods, including the Gerchberg-Saxton algorithm and the hybrid input-output algorithm, have been successfully demonstrated for computer simulations of Cu_3Au and show early promise for reconstruction of domain structure from real measurements. Data obtained at the Advanced Photon Source beamline 33-ID-D at 8.5 keV are presented, and the requirements for successful reconstruction of images from such data are discussed.

Keywords: coherent x-ray diffraction, Cu_3Au, phase retrieval

1. INTRODUCTION

The recent availability of high-brilliance x-ray beams has made it possible to extend many coherent techniques which have traditionally utilized laser light into the x-ray regime. Since these high-brilliance sources do not have the intrinsic coherence properties of a laser, it is necessary to pass the x-ray beam through a pinhole or through slits which have a dimension smaller than or on the order of the lateral (spatial) coherence length of the beam.[1] As a result, to obtain a coherent x-ray beam costs a great deal in flux. However, the use of a coherent beam makes measurements sensitive to specific local sample structures rather than only their ensemble-averaged statistical properties.

While this paper concerns a developing technique which involves the acquisition of static "snapshot" measurements of the scattered coherent x-ray beam, there have been several successful experiments to measure the time autocorrelation function of the scattered beam in order to obtain characteristic fluctuation or decay times within the sample.[2–6] Though the measurements required for such dynamical experiments share many similarities with those described below, the goal is quite different. The technique we describe here has as its goal the retrieval of the phase of the scattered beam for the purpose of generating a real-space image of the sample. This type of microscopy, essentially the extension of x-ray crystallography to nonperiodic samples, has an ideal-case resolution limit of the x-ray wavelength, e.g. $\sim$1 Å in the case of hard x-rays, but in practice is determined by exposure time or sample damage.[7]

2. Cu_3Au ANTIPHASE DOMAINS

2.1. Real-Space Structure

The binary alloy Cu_3Au has been of interest for x-ray diffraction studies due to its strong scattering and its well-ordered crystal structure. The unit cell of Cu_3Au is face-centered cubic, with copper on the face sites, and gold on the corner sites. The sample thus consists of planes which contain alternately all copper or half-copper, half-gold. A low-energy type of domain boundary can be formed by swapping the positions of copper and of gold in one of the half-copper, half-gold planes, and continuing the resulting stacking sequence in the direction normal to that plane. There are, as a result, four equivalent domains of Cu_3Au which differ only in a phase shift from one another; hence, they are referred to as antiphase domains (APDs). Above the critical temperature, T_c = 668K, only short-range

ordering of the domains exists. While annealing just below T_c, the APDs increase in size and exhibit long-range ordering.[8] The antiphase boundaries (APBs) have been observed to prefer certain crystallographic directions, but do not strictly follow them.[9] A typical annealing schedule of a few days just below T_c results in APDs measuring tens to hundreds of nanometers.

The Cu_3Au sample which we used for the measurment described in this paper was a ~2000 Å thin film with a (111) surface orientation, grown on sapphire. Conventional x-ray diffraction measurements showed that the APDs had an average size of 1000 Å.

2.2. Reciprocal-Space Structure

Long-range ordering in Cu_3Au gives rise to superstructure Bragg reflections with mixed even and odd hkl, with a scattering factor given by

$$F = S(f_{Au} - f_{Cu}), \tag{1}$$

where S is the long-range order parameter and f is the atomic scattering factor. For a completely disordered structure, $S = 0$, and for a completely ordered structure with no APBs, $S = 1$. At a given superstructure reflection, two of the four types of APDs will have a phase shift of π relative to the other two. The reflection from one APD, which has $S = 1$ within its boundaries, introduces in the beam a phase shift of either 0 or π relative to that of a neighboring APD, but the amplitude of reflection does not depend on which type of domain is involved. If the beam does not penetrate deeper than the domain size, or if the domains extend throughout the crystal, then the sample can be considered a 2-dimensional random array of APDs. A beam reflecting from the surface of such a crystal, oriented at a superstructure reflection, is presented with what is essentially a mirror with a phase-modulated texture. If the beam illuminating the sample is coherent, the reflection in the far-field becomes a speckle pattern, the details of which depend on the specific APD structure within the illuminated portion of the sample.[10] See Figure 1 for an example.

3. MEASURING COHERENT X-RAY DIFFRACTION

The Cu_3Au coherent x-ray diffraction measurement we describe was carried out at beamline 33-ID-D at the Advanced Photon Source (APS). The beamline consists of an APS Undulator A which has source sizes of $\sigma_x \approx 350$ μm in the horizontal and $\sigma_y \approx 50$ μm in the vertical.[11] At the sample position, a distance $D = 40$ m from the source, the beam is suitably coherent over a transverse distance

$$\xi_{x,y} = \frac{\lambda D}{2\sqrt{\pi}\sigma_{x,y}}, \tag{2}$$

where λ is the x-ray wavelength.[12] At 8.5 keV, we have $\lambda = 1.46$ Å, $\xi_x \approx 4.7$ μm, and $\xi_y \approx 33$ μm.

A double-crystal Si(111) monochromator yields a beam with $\Delta E/E \approx 2 \times 10^{-4}$, where E is the beam energy and ΔE is the full-width-at-half-maximum (FWHM). This yields a longitudinal (temporal) coherence length $\xi_{\|} = \lambda^2/\Delta\lambda \approx 7300$ Å. The speckle contrast in the experiment is expected to degrade if an optical path length difference (PLD) greater than $\xi_{\|}$ is introduced. This can be avoided in a reflection-geometry experiment if the penetration depth into the sample is limited or if the sample is thin. For the measurement reported here, the penetration depth is greater than the thickness of the Cu_3Au film, but the film is thin enough that we have $PLD \leq 500$ Å.

A crossed pair of slits with a novel roller-blade design serve two purposes in the experiment: to select a coherent portion of the incoming (incoherent) beam, and to define the edges of the beam which propagates to the sample. Each slit consists of a pair of highly polished molybdenum rollers which are oriented parallel to one another and clamped together with a 100 μm shim separating them, forming a gap for the x-ray beam to pass. The pair of rods are then tipped about the rods' axis to pinch off the beam. A long lever arm to the actuator gives this motion sufficient precision to allow greater than 1 μm precision slit gap settings from zero to tens of micrometers in a reproducable fashion.

The design of the slits does lead to an asymmetry, in that the apparent gap of the slits depends on the direction from which they are viewed. This can be clearly seen in the Fraunhofer pattern in Figure 2 and is described in detail in another paper.[13] Measuring the Fraunhofer pattern is expected to be significant for the calculation of the sample illumination distribution, $B(x, y)$, which is critical in applying the phase retrieval methods described below.

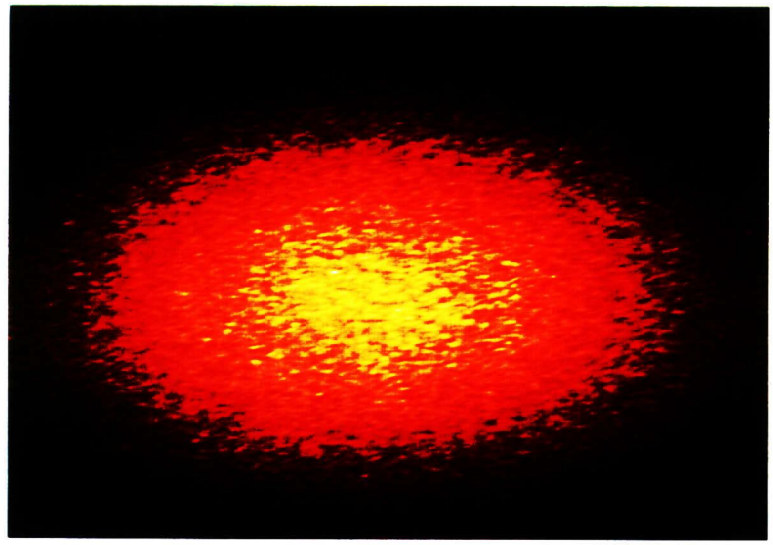

Figure 1. Example of a measured Cu_3Au speckle pattern. Acquired at 8.5 keV with 10 accumulations of 104 s, the image shown measures 706 pixels by 496 pixels, or 15.9 mm by 11.2 mm. (Each pixel has an angular extent of 7.6 μrad.).

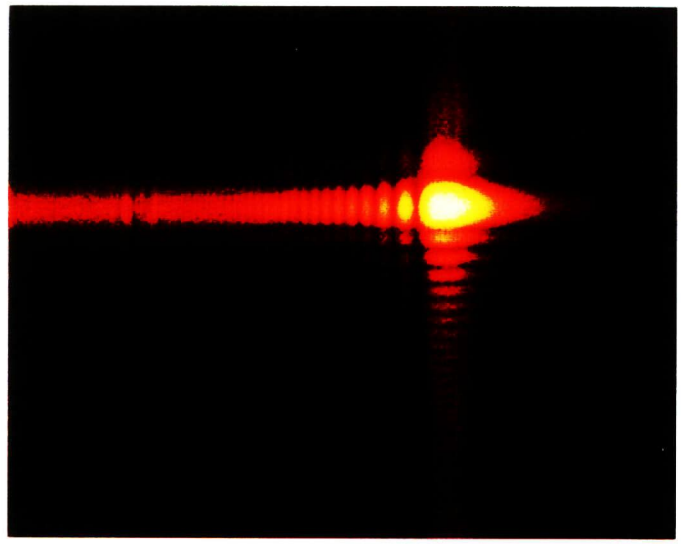

Figure 2. Example of Fraunhofer diffraction from the roller-blade slits at 6.875 keV, measured 2.95 m away, with 10 accumulations of 7 s each. The image shown measures 624 pixels by 496 pixels. The asymmetry of the pattern results from the parallax effect due to the slit design.

We used a standard Huber 4-circle diffractometer to orient the sample and detector. The sample was mounted 20 mm from the vertically closing slit and 87 mm from the horizontally closing slit. These distances were minimized so that the spot size on the sample would be as small as possible.

The detector, obtained from Princeton Instruments, was a deep-depletion EEV CCD of 1152 × 1242 pixels each 22.5 μm on a side, thermoelectrically cooled to -50°C and directly illuminated by the x-ray beam. At 8.5 keV, the quantum efficiency of the CCD was measured to be around 20 percent. The detector was mounted at a distance of 2.95 m from the sample position.

4. PHASE RETRIEVAL METHODS

4.1. Gerchberg-Saxton Error Reduction Algorithm

One of two algorithms we apply to retrieve the phases of a speckle pattern is the Error Reduction (ER) algorithm due to Gerchberg and Saxton.[14,15] We apply the algorithm in a straightforward way, based on the following model of the coherent diffraction process. The coherent x-ray beam propagates from the slits to the sample by Fresnel diffraction, resulting in a wavefront having a complex amplitude given by the expression

$$B(x,y)e^{i\phi_0(x,y)}\,, \tag{3}$$

where $B(x,y)$ is the real amplitude of the wavefront at the sample position and $\phi_0(x,y)$ describes its phase. After reflection from the phase-modulating sample surface, an additional position-dependent phase $\phi_s(x,y)$ is introduced which, in the case of Cu_3Au APDs, takes on the distinct values 0 and π. Therefore, immediately after reflection from the sample surface, the wavefront is described by the real-space complex amplitude $f(x,y)$, where we have

$$f(x,y) = B(x,y)e^{i[\phi_0(x,y)+\phi_s(x,y)]}\,. \tag{4}$$

The beam subsequently propagates according to the Fourier transform into the far field, where we obtain the reciprocal-space complex amplitude

$$F(q_x,q_y) = \sqrt{I(q_x,q_y)}e^{i[\phi_I(q_x,q_y)]}\,, \tag{5}$$

where $I(q_x,q_y)$ is the real-valued speckle pattern intensity measured in the experiment and $\phi_I(q_x,q_y)$ is the phase of the wavefront at the detector, which is not measured.

We start the algorithm with the array describing the real-space initialized to $B(x,y)$ with randomized phases uniformly distributed on the interval $[0,2\pi]$. The FFT is applied to the array to obtain an estimate, $F_0(q_x,q_y)$, of the reciprocal-space wavefront. The amplitude of F_0 is replaced by the measured amplitude $\sqrt{I}$, leaving the phase unchanged. The inverse FFT is then applied to obtain an estimate of the real-space wavefront, f_1. The amplitude of f_1 is replaced by the calculated illumination envelope B, again leaving the phase unchanged. The process is then repeated, and each f_n forms the estimate of the real-space wavefront. At each iteration, the progress of the convergence is tracked by computing the following error metric:

$$R_n = \frac{\sum_{\mathbf{h}}(f_n - B)^2}{\sum_{\mathbf{h}} B^2}\,, \tag{6}$$

where the summation on $\mathbf{h}$ runs over the whole array. In iterating the ER algorithm, we find that the error metric decreases but that the solution often stagnates in a manner which has been observed and addressed by others.[16]

4.2. Hybrid Input-Output Algorithm

In order to overcome the problem of stagnation in the phase retrieval process, we have implemented an adaptation of the Hybrid Input-Output (HIO) algorithm as described by R. P. Millane and W. J. Stroud.[16,17] The strength of the HIO algorithm is that it provides a means for supplying more information about the true image f, by mixing f_n with a constrained version of itself before the FFT is applied to obtain F_n. The reciprocal-space part of the algorithm is the same as that of the ER algorithm.

We use the constraint that the real-space wavefront is of the form

$$c_n(x,y) = \begin{cases} \min\left(B(x,y),|f_n(x,y)|\right)e^{i\phi_0(x,y)} & \text{if} \quad \mathrm{Re}(f_n(x,y)e^{-i\phi_0(x,y)}) \geq 0 \\ -\min\left(B(x,y),|f_n(x,y)|\right)e^{i\phi_0(x,y)} & \text{if} \quad \mathrm{Re}(f_n(x,y)e^{-i\phi_0(x,y)}) < 0 \end{cases}\,. \tag{7}$$

This expression forces the wavefront to have a phase which matches the constraint resulting from the APD structure of Cu_3Au. The amplitude of the wavefront at each point is allowed to be less than B, such that the point may cross smoothly from representing one type of domain to the other.

The HIO algorithm does not always cause R to decrease in the case of the above constraint; however, a sharp decrease in R while iterating the HIO algorithm can be taken as a sign that the algorithm is finding an acceptable solution. Switching to the ER algorithm does not drive the system away from such a solution but, instead, refines the solution further.

5. PHASE RETRIEVAL ON SIMULATED SPECKLE DATA

As a test of the ER and HIO algorithms, we have constructed a simulation of a 2-dimensional APD structure using a simple Metropolis algorithm model of domain coarsening. The simulation does not include any physical parameters which would case the APBs to prefer certain orientations; as such, it is not expected to give a particularly accurate picture of an actual Cu_3Au APD texture. However, it should serve the purpose of testing the constraint described above. See Figure 3.

The use of oversampling to solve the phase problem uniquely is well-known;[18,19] however, the introduction of various types of constraints via the HIO algorithm can be expected to have an impact on the degree of oversampling or on the number of iterations of the algorithm needed to converge to a correct image. We sought to examine the effect of varying the degree of oversampling on the convergence of the ER and HIO algorithms when applied to the simulation. The 128 $\times$ 128 real-space array illustrated in Figure 3 was padded by some ratio with zeroes so that its Fourier transform became oversampled by the same ratio. For each oversampling ratio, 50 independent fits starting with different random starting phases were run with three cycles of 200 iterations of HIO and 100 iterations of ER. Figure 4 shows the reconstructed image with the lowest R for five levels of oversampling. Note that the major features have been reconstructed for the images with an oversampling ratio greater than $2\times$ (images (B)-(D)), but note also that only image (B) has been oversampled by $2\times$ in each dimension. Similar results of oversampling, but with a different type of constraint, have been reported by J. Miao, D. Sayre, and H. N. Chapman.[19] The fidelity of image (B) is much better than that of images (C) and (D), as it retains even the single-pixel domains near the center of the image. However, further iterating on images (C) and (D) may cause them to converge to a similar level. An indicator for convergence as in image (B) is that R begins to drop during the HIO iterations, as shown in Figure 5. Figure 6 shows the terminating values of R for all 50 fits for each oversampling configuration. The general shape of the curves for the configurations which better reconstructed the test APD structure differs near the low-R end from the two which do not; a rolloff is evident for the more highly oversampled configurations which extends further to the right as the degree of oversampling increases. Thus, a competition exists between the number of independent fits required to find a successful reconstruction and the size of the array (and, hence the computing time) for each fit.

6. RECONSTRUCTION OF IMAGES FROM THE MEASUREMENTS

The ER and HIO algorithms were then applied to the actual Cu_3Au coherent diffraction measurement shown in Figure 1. This image has speckles extending over a much greater range of reciprocal space, relative to the size of the speckles, than does the simulated image. As a result, the length scale of the APDs within the illuminated area of the sample must be quite small in relation to the size of the whole illuminated area, which presents the problem that the array size used in the reconstruction must be quite large in order to preserve the oversampling ratio expected to be necessary for successful reconstruction, and still have the APDs in the reconstructed image span more than a few pixels. This problem can be addressed by reducing the size of the beam footprint on the sample or by replacing the sample with one having larger APDs. Also, the noise in the measurement may cause difficulty in obtaining successful image reconstructions. The peak intensity in the measurement shown in Figure 1 records only $\sim$700 photons, so that the regions of the speckle pattern with much lower intensity will have considerable statistical noise. Other investigations regarding solution of the phase problem in the presence of noise have been reported.[20] A third possible difficulty in reconstructing real-space images of the APDs in such speckle patterns is that the beam impinging on the sample is not purely coherent, since the horizontal coherence length of the beam is nearly the same as the horizontal slit opening. As as result, the speckle pattern recorded on the CCD is not strictly the Fourier transform of the wavefront at the sample as it is modelled by the reconstruction algorithms. We are presently evaluating the requirements for image reconstruction in view of these issues, and work on reconstructing images from the measured speckle patterns is in progress.

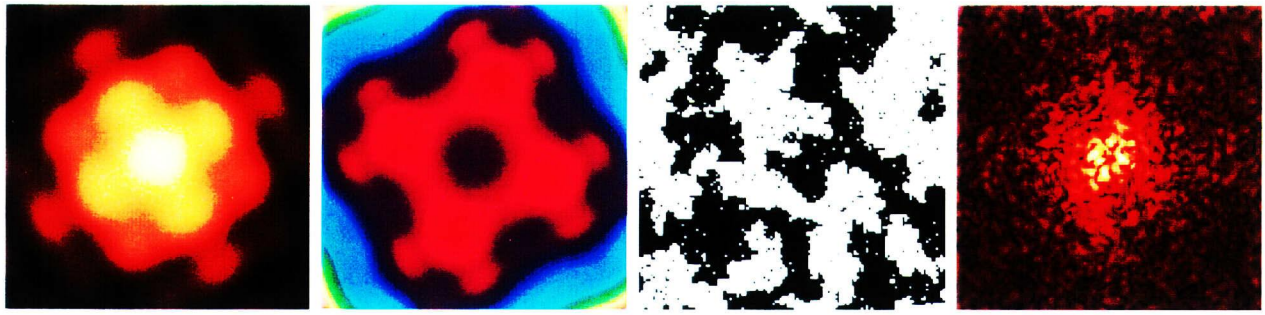

Figure 3. Real-space Fresnel diffraction amplitude of the simulation (left), Fresnel contribution to the real-space phase (left center), APD structure simulation (right center), simulated speckle pattern (right). The three real-space images show the entire 128×128 array, while the speckle pattern shown is the central 128×128 region in a 256×256 oversampled speckle pattern computed from the same real-space image. A cyclic red-blue-green-red color triangle is used to represent phases from 0 to 2π.

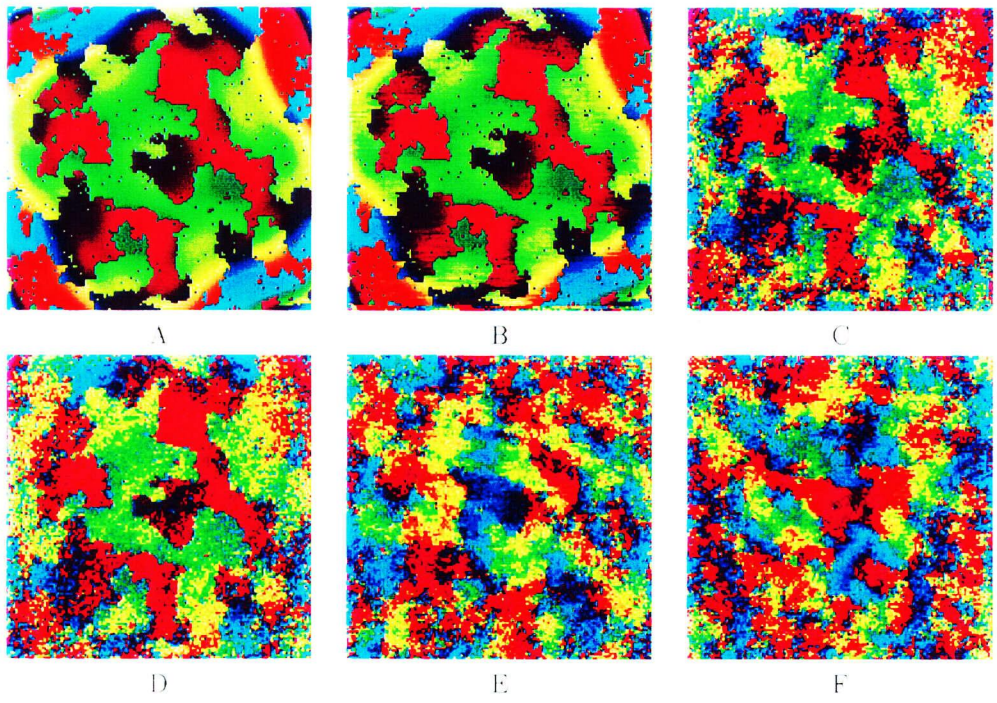

Figure 4. Plots of the phase over the region from Figure 3: (A) the Fresnel+APD phase used to generate the simulated speckle pattern, (B) the phase of the lowest-R reconstruction after padding to 256×256, (C) 192×192, (D) 128×256, (E) 160×160, and (F) no padding. Plots have been adjusted for constant phase factors and duals, which are ambiguous for the fit.

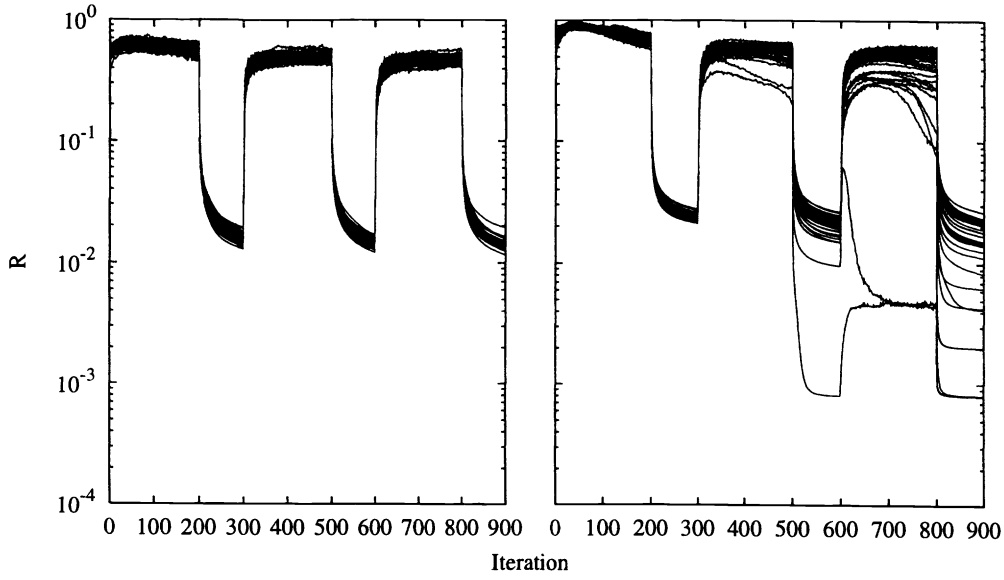

Figure 5. Log of R as 50 fits converge for the case of a 160×160 image (left) and for the case of the same image data padded with zeroes to form a 256×256 image, corresponding to a 2× oversampling in each dimension (right).

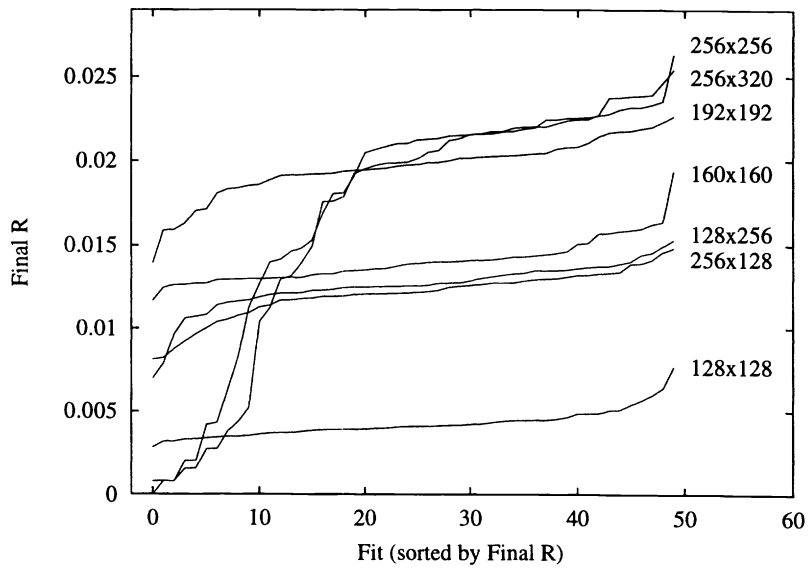

Figure 6. Terminal values of R for 50 independent fits for a series of zero-padding configurations. The fit numbers have been sorted on the terminal values of R and do not represent the actual ordering of the 50 outcomes. The shape of the curves should be representative of the distribution in R for a much larger ensemble of fits. Note the markedly different behavior for the convergence of the 256×256 and 256×320 images compared to the others. Since R does scale with array size, it should not be used for comparing the quality of reconstruction for differing array sizes; even though the lowest-R 192×192 image compares favorably with the lowest-R 160×160 image, the latter has the lower R.

7. SUMMARY AND FUTURE DIRECTIONS

An experimental technique for the measurement of speckle patterns using coherent hard x-rays with sufficient stability, resolution, and intensity has been demonstrated at the APS. Cu_3Au, because of its APD structure and the concomitant constraints on any reconstructed image, makes a convenient test sample for developing coherent x-ray diffraction as a means of doing real-space microscopy. The problem of retrieving the phase of the scattered beam has been studied numerically using a range of oversampling ratios, and it appears that oversampling only by a factor of two, rather than by a factor of 2^2, may be sufficient for successful image reconstruction, at least with the use of the APD constraint. However, the rate of convergence and the fidelity of the image was seen to improve as the oversampling ratio exceeded four. The speckle patterns from Cu_3Au which have been measured experimentally at this time have much more complexity than those in the simulations, and will require much more computational effort to invert into real-space images. Even then, there may be difficulties resulting from measurement noise and from the incoherent contribution to the scattering. Future simulations will seek to map out the requirements, at least with respect to the acceptable level of noise in the measurements.

ACKNOWLEDGMENTS

We are grateful for the assistance of P. Zschack and P. Jemian at the UNICAT 33-ID beamline. The UNICAT facility located at the APS is supported by the University of Illinois, Materials Research Laboratory, the Oak Ridge National Laboratory, the National Institute of Standards and Technologies, and UOP Research & Development. The APS is supported by the U.S. Department of Energy, BES, Office of Energy Research, under contract No. W-31-109-ENG-38. We would like to acknowledge R. Millane for valuable discussions C. P. Flynn and R. Appleton for providing us with the Cu_3Au sample. One of us, J. Pitney, wishes to acknowledge fellowship support from the U.S. National Science Foundation (NSF) under grant number DGE93-54978. This work was supported by the NSF under project number DMR98-76610.

REFERENCES

1. M. Born and E. Wolf, *Principles of Optics*, Pergamon Press, Oxford, 1980.
2. S. Brauer, G. B. Stephenson, M. Sutton, R. Brüning, E. Dufresne, S. G. J. Mochrie, J. Als-Nielsen, G. Grübel, and D. L. Abernathy, "X-ray intensity fluctuation spectroscopy observation of critical dynamics in Fe_3Al," *Phys. Rev. Lett.* **74**, pp. 2010–2013, 1995.
3. S. B. Dierker, R. Pindak, R. M. Fleming, I. K. Robinson, and L. Berman, "X-ray photon correlation spectroscopy study of brownian motion of gold colloids in glycerol," *Phys. Rev. Lett.* **75**, pp. 449–452, 1995.
4. T. Thurn-Albrecht, W. Steffen, A. Patkowski, G. Meier, E. W. Fischer, G. Grübel, and D. L. Abernathy, "Photon correlation spectroscopy of colloidal palladium using a coherent x-ray beam," *Phys. Rev. Lett.* **77**, pp. 5437–5440, 1996.
5. S. G. J. Mochrie, A. M. Mayes, A. R. Sandy, M. Sutton, S. Brauer, G. B. Stephenson, D. L. Abernathy, and G. Grübel, "Dynamics of block copolymer micelles revealed by x-ray intensity fluctuation spectroscopy," *Phys. Rev. Lett.* **78**, pp. 1275–1278, 1998.
6. O. K. C. Tsui and S. G. J. Mochrie, "Dynamics of concentrated colloidal suspensions probed by x-ray correlation spectroscopy," *Phys. Rev. E* **57**, pp. 2030–2034, 1998.
7. D. Sayre and H. N. Chapman, "X-ray microscopy," *Acta Cryst. A* **51**, pp. 237–252, 1995.
8. B. E. Warren, *X-ray Diffraction*, Addison-Wesley Publishing, Reading, Mass., 1969.
9. P. Hirsch, A. Howie, R. B. Nicholson, D. W. Pashley, and M. J. Wheelan, *Electron Microscopy of Thin Crystals, Second Revised Edition*, Robert E. Krieger Publishing, Malabar, Fla., 1977.
10. M. Sutton, S. G. J. Mochrie, T. Greytak, S. E. Nagler, L. E. Berman, G. A. Held, and G. B. Stephenson, "Observation of speckle by diffraction with coherent x-rays," *Nature* **352**, pp. 608–610, 1991.
11. Z. Cai, R. J. Dejus, P. D. Hartog, Y. Feng, E. Gluskin, D. Haeffner, P. Ilinski, B. Lai, D. Legnini, E. R. Moog, S. Shastri, E. Trakhtenberg, I. Vasserman, and W. Yun, "APS undulator radiation - first results," *Rev. Sci. Instrum.* **67**, p. 3348, 1996.
12. J. W. Goodman, *Statistical Optics*, John Wiley and Sons, New York, 1985.
13. J. L. Libbert, J. A. Pitney, and I. K. Robinson, "Asymmetric Fraunhofer diffraction from roller-blade slits," *J. Synch. Rad.* **4**, pp. 125–127, 1997.

14. R. W. Gerchberg and W. O. Saxton, "A practical algorithm for the determination of phase from image and diffraction plane pictures," *Optik* **35**, pp. 237–246, 1972.
15. J. R. Fienup, "Phase retrieval algorithms: a comparison," *Appl. Opt.* **21**, pp. 2758–2769, 1982.
16. J. R. Fienup and C. C. Wackerman, "Phase-retrieval stagnation problems and solutions," *J. Opt. Soc. Am. A* **3**, pp. 1897–1907, 1986.
17. R. P. Millane and W. J. Stroud, "Reconstructing symmetric images from their undersampled Fourier intensities," *J. Opt. Soc. Am. A* **14**, pp. 568–579, 1997.
18. R. H. T. Bates, "Fourier phase problems are uniquely solvable in more than one dimension. I. underlying theory," *Optik* **61**, pp. 247–262, 1982.
19. J. Miao, D. Sayre, and H. N. Chapman, "Phase retrieval from the magnitude of the Fourier transforms of nonperiodic objects," *J. Opt. Soc. Am. A* **15**, pp. 1662–1669, 1998.
20. R. H. T. Bates, W. R. Fright, and P. H. Gardenier, "Gerchberg-Saxton phase retrieval when image magnitude given only approximately," in *Digital Image Recovery and Synthesis*, P. S. Idell, ed., *Proc. SPIE* **828**, pp. 171–176, 1987.